Cement and Concrete Research 137 (2020) 106195

Contents lists available at ScienceDirect

Cement and Concrete Research

journal homepage: www.elsevier.com/locate/cemconres

Fibrillar calcium silicate hydrate seeds from hydrated tricalcium silicate lower cement demand

Jiaqi Li*, Wenxin Zhang, Ke Xu, Paulo J.M. Monteiro

Department of Civil and Environmental Engineering, University of California, Berkeley, Berkeley, CA 94720, United States

ARTICLE INFO

Keywords:
C-S-H
Green additive
XANES
Tomography
Life-cycle assessment

ABSTRACT

Debates remain on the influencing factor and long-term performance of C-S-H-seeded paste. In this study, phase-pure seeds were prepared from diluted Ca_3SiO_5 hydration. The seed structures were determined using synchrotron-based X-ray diffraction, X-ray absorption spectroscopy, and transmission electron microscopy. Nanofoils and similar Ca and O environments were present in seeds of different Ca/Si; nanofibers were present in high-Ca seeds only which showed lower silicate polymerization. Calorimetry and setting results showed a greater hydration acceleration with high-Ca seeds; seed shape dominated the acceleration. 0.5 wt% high-Ca seeds increased 1- and 28-days paste strength by 300% and 20%, respectively. Life-cycle assessment showed negligible (< 1%) influence of seeds on energy demand and CO_2 emissions of the paste production. The CO_2-intensity normalized by strength of seeded pastes decreases by ~25% at 28 days. This study sheds light on the use of C-S-H seeds from waste concrete and wash water, as a means of lowering cement demand.

1. Introduction

Global Portland cement (PC) production is ~4.1 Bt/yr, which corresponds to ~9% global anthropogenic CO_2 emissions and ~7% primary energy consumption [1,2]. Reducing cement content in concrete is the most efficient approach to lowering the environmental impacts of concrete production [3]. However, productions of conventional cement substitutes, e.g., coal fly ash (~300 Mt/yr) and granulated blast-furnace slag (GBFS, ~300 Mt/yr), never meet the massive demand for cement-based materials (e.g., concrete of > 30 Bt/yr demand [2]). Furthermore, the pursuit of renewable energy resources has threatened the supply chain of fly ash from coal-fired power plants. Besides the promising calcined clay-limestone system [4], other cement substitutes are either of low-reactivity (e.g., volcanic ash) or of low-availability (e.g., diatomite, rice husk ash, and silica fume) [5–7]. Such low reactivity results in lower strength of concrete, particularly at the early age [8], conflicting economic interests of the construction industry. The 28 day compressive strength is a critical index for structural design, therefore higher 28 day-strength ensures eco-friendliness by the possibility of concrete structures having smaller cross-section, e.g., in column designs.

Calcium silicate hydrate (C-S-H) is the primary binding phase in PC-based concrete [9]. C-S-Hs are porous nano-crystallites with a defected structure similar to tobermorite [10–15]. Pure C-S-H can be synthesized by the lime-silica reaction, sol-gel method, or co-precipitation [10,16], and the synthetic C-S-H seeds are foil-like or globular [17]. Recent studies show that the addition of synthetic C-S-Hs can significantly improve the strength of cement paste, mortar, and concrete at 1–3 days by providing a large number of nano-nucleation sites (seeds) and growth templates for the hydration products of cement [10,18,19]. However, the influence of C-S-H seeds on the long-term performance of cement remains a matter of debate. Higher, lower, and comparable strengths of seeded cement/mortar compared to the reference groups at 28 days were all reported [20]. John et al. [21] suggested that C-S-H increased the compressive strength of paste at 28 days, and fresh seeds at Ca/Si 0.8 exhibited higher strength improvement than seeds at Ca/Si of 1.2. Wang et al. [22] suggested that 1 wt% C-S-H seeds had negligible influences on strength at 28 days while 2 wt% C-S-H slightly decreased compressive strength at 28 days. Owens et al. [23] suggested that C-S-H seeds at 2 wt% and 4 wt% level decreased the strength at 28 days. The contradictory results can be attributed to the impurities (unreacted SiO_2 at low Ca/Si or secondary product $Ca(OH)_2$ at high Ca/Si), degradation (carbonation products) of the seeds, or the lack of characterization of C-S-H seeds [20,21,24].

The sale prices of precursors ($Si(C_2H_5O)_4$, silica fume, and Na_2SiO_3) of the seeds used in these syntheses are hundreds/thousands of US$ per tonne due to their limited production/co-production or associated intense energy demand [10,25]. Besides the aforementioned uncertain

* Corresponding author at: 115 Davis Hall, University of California, Berkeley, CA 94720, United States.
E-mail address: Jiaqi.li@berkeley.edu (J. Li).

https://doi.org/10.1016/j.cemconres.2020.106195
Received 14 June 2020; Received in revised form 24 July 2020; Accepted 30 July 2020

long-term performance of seeds, these external factors can limit the wide use of C-S-H seeds as well. To put a perspective, as the price of ordinary Portland cement is only $120/t, the massive demand for cement (4.1 Bt/yr) leads to great sensitivity to the cost of seeds.

As C-S-H in concrete forms from the hydration of Ca_3SiO_5 (C_3S) and Ca_2SiO_4 (C_2S), the major compounds in PC, seeds can be massively manufactured by hydrating C_3S and/or C_2S. Efficient seeds from hydrated C_3S or PC can significantly lower the seed cost and improve the sustainability of cement-based materials. These hydration product C-S-Hs, mainly from C_3S hydration [26], are typically fibrillar and often intermix $Ca(OH)_2$ [27,28]. Previous studies mainly focused on the influence of dosage and compositions of foliar/globular seeds on the hydration acceleration and strength development [20]. The influences of fibrillar seeds on the cement hydration and performance have not been explored yet.

Although seeded paste/mortar/concrete may present higher strength [10], the sustainability of cement/mortar/concrete is essentially relevant to the environmental impacts and energy requirement of the materials production. Life Cycle Assessment (LCA) is widely recognized as a reliable tool for decision-makers to manage waste materials and to priorate resource use in the environmental aspects. Previous LCA studies estimated energy consumption and greenhouse gas (GHG) emissions of cement-based materials blended with industrial by-products or natural resources [8,29–32]. However, the energy demand and GHG emissions of the production of seeded cement-based materials have rarely been studied.

In this study, phase-pure C-S-H seeds with fibrillar and foil-like morphology were synthesized by diluted-hydration of triclinic C_3S. The chemistry of the seeds was characterized using X-ray absorption near-edge structure (XANES) spectroscopy at Ca L-, O K-, and Si K- edges, and synchrotron-radiation based X-ray diffraction (XRD). The morphology of the seeds was determined using scanning transmission soft X-ray spectroscopy (STXM) and high-resolution transmission electron microscopy (TEM). The acceleration effects of the seeded cement pastes were measured using isothermal calorimetry and synchrotron-radiation based X-ray microtomography. The setting time, compressive strength at 28 days, and pore structures of seeded pastes were determined. The energy consumption and GHG emissions of manufacturing seeds and seeded pastes were modeled using LCA. Additionally, the study discusses the implications in the use of C-S-H reclaimed from recycled cement-based materials.

2. Materials and experiments

2.1. Materials

Triclinic Ca_3SiO_5 (Mineral Research Processing, passed by 5um-sieve) was mixed with deionized water at liquid-to-solid ratios (l/s) of 324 and 910 for the synthesis of HighCa and LowCa C-S-H seeds, respectively. After equilibrium at 25 °C, the solutions were filtered using 0.45 μm nylon filters (Acrodisc). The filtered seeds were used freshly for cement pastes preparation. For characterization studies, the filtrates were mixed with 99 + % isopropanol at ~5 °C at l/s of 30, filtrated, and analyzed immediately or stored under N_2 protection until analysis. For mass measurement of the dry seeds, the wet seeds were dried in vacuum for 7 days. From 1 g of precursor, i.e., C_3S, either 0.54 g HighCa or 0.40 g LowCa seed was yielded.

2.2. Experiments

X-ray absorption imaging and spectroscopy. The XANES spectra and transmission images (25-nm resolution) at Ca $L_{2,3}$- and O K- edges were obtained using the scanning transmission soft X-ray spectroscopy (STXM) at the beamline 5.3.2.2 at the Advanced Light Source (ALS) in the Lawrence Berkeley National Laboratory. The filtered seeds were dispersed in 99 + % isopropanol at ~25 °C, then dropped onto a SiN membrane window (100 nm thick). The windows were placed on the STXM sample stage at 1/3 atm.

The XANES spectra at Si K-edge were collected at the PHOENIX beamline at the Swiss Light Source using fluorescence-yield mode with a beam size of 500 μm × 500 μm. Thin layers of dry seeds were mounted on indium foils and then attached to a copper plate. The plate was mounted on a sample stage in a vacuum chamber.

2.2.1. TEM

A high-resolution TEM (ThemIS coupled with Bruker SuperX energy-dispersive X-ray spectroscopy (EDS) detector) was used to collect images and EDS results under laboratory conditions. The filtered seed was dispersed in 99 + % isopropanol, followed by sonication for 1 min. The seeds samples were then dropped onto copper TEM grids (Lacey-carbon film).

2.2.2. XRD

The XRD experiment was conducted at the beamline 12.2.2 of the ALS. The incident X-ray beam energy was 25 keV with a beam size of ~30 μm. The sample-to-detector (MAR345 image plate) was ~330 mm. Dry seeds were loaded into fine glass capillaries for XRD. The exposure time of the sample was 810 s. Lattice constants were refined using *CelRef* with Merlino's B11m tobermorite structure [33].

2.2.3. Surface area

The specific surface area measurements of the dried seeds were performed using a BET multipoint (6 points isotherm) N_2 physisorption device (TristarII 3020, Micromeritics). Before the measurement, the dry seeds were degassed in an external degassing station (VacPrep 061, Micromeritics) at 40 °C with N_2 flow for 16 h. More details can be found in [34].

2.2.4. Concentration

C_3S suspension was filtered using 0.45 μm nylon filters. The filtrates were diluted in 2 wt% HNO_3. The Ca concentration of the acidified suspension was measured using a Perkin Elmer inductively coupled plasma–optical emission spectrometry (ICP-OES). Standard solutions were prepared by diluting standards (Inorganic Ventures) in 2 wt% HNO_3 solution.

2.2.5. Calorimetry

All cement pastes were prepared at a water-to-binder ratio (w/b) of 0.5 at 23 °C. The seeds were dispersed in deionized water, then sonicated for 2 min. Subsequently, 0.5 wt% (by cement mass) seeds slurry was mixed with ASTM type I cement for 3 min. ~5 g paste was mounted into a plastic ampoule, then loaded into an isothermal calorimeter (TAM Air, TA Instruments) at 25 °C. During the first hours of cement hydration, heat flow evolution is linear and correlates to the hydration rate of silicates and the growth of C-S-H. The hydration acceleration is represented by the change in derivative of heat flow with respect to time. The relative acceleration is defined as the ratio of slope of the linear range of a seeded paste over that of the reference paste [35].

2.2.6. Microtomography

The synchrotron-radiation based X-ray microtomography was conducted at the beamline 8.3.2 of the ALS. The beam energy was set to 35 keV with a constant beam current of 500 mA during the scans. 1969 projections with an angle step of 0.09° and an exposure time of 20 ms each were acquired on a 5× Mitutoyo magnification optical lens with a spatial resolution of 1.3 μm/voxel and a 2560px PCO_Edge CCD camera a field of view of 3.3 mm. The mixed pastes (w/b = 0.5) were loaded into thin-wall polyimide tubing (3 mm diameter) and sealed with fast setting epoxy at 25 °C. At 3 h and 8 h, the filled tubes were placed into the sample holder of the beamline at ~25 °C. Reconstructed slices (tomograms) were computed using the filtered back projection algorithm on Tomopy [36,37] at the ALS.

2.2.7. Performance

0.5 wt% sonicated seed slurry was added into cement (w/b = 0.5), followed by mixing at 136 RPM for 2 min and 281 RPM for 2 min using a Hobart N50 mixer at 25 °C. Setting time of cement pastes was determined by Vicat needle penetration tests per ASTM C191. For strength measurement of pastes, the pastes (w/b = 0.5) were loaded into 25.4 mm × 25.4 mm cylindrical molds, then cured in water at 25 °C until analysis. At 28 days, the pastes samples were sawed, treated with isopropanol to stop hydration, and dried in a N_2-filled oven at 40 °C. The porosity measurements of hardened pastes at 28 days were performed using an AutoPore IV 9500 porosimeter (maximum pressure 200 MPa).

3. Life-cycle assessment

The life cycle model built following the ISO 14044 standards includes raw material extraction, production/processing, transportation to concrete plant, and paste mixing/batching. A cradle-to-gate model was developed for transportation (25 km on road for raw materials from extraction to a cement plant plus 100 km on road for cement and C_3S (or alite) from the cement plant to a concrete plant) and the production of cement and seeds (Fig. 1). The functional unit in this LCA study is 1 m^3 seeded/unseeded paste.

We assumed that a preheater/precalciner kiln was used for producing both cement clinker and the seed precursor in a California scenario. The seed precursor in this LCA is assumed to be alite, monoclinic C_3S, not pure triclinic C_3S. This is because 1) alite, not triclinic C_3S, is the major phase in PC; 2) the production of pure triclinic C_3S used in our experimental work requires highly pure raw materials and high kilning temperature and the scale-up of triclinic C_3S production is not practical; 3) the raw materials assumed in the LCA study are not pure; ($CaCO_3$ content in modeled limestone is 93.5%); 4) the required dopant, e.g., MgO, content in alite is low, just ~1.5% [38]. A US average kiln fuel mix was modeled to be used (more details in Supporting Information). A net reaction enthalpy of 1.76 MJ is required to produce per kg of clinker. However, the average thermal requirement of clinker production in a preheater/precalciner kiln is 3.3 MJ/kg of clinker [31], and the process-based CO_2 emission is assumed to be 0.522 kg/kg of clinker produced. The net reaction enthalpy of alite (C_3S) formation is 1.84 MJ/kg of C_3S/alite produced, and the process-based CO_2 emission is 0.579 kg/kg; we accounted for the higher net enthalpy of C_3S/alite production compared to clinker through an increase in thermal energy demand [29] (see SI). Note that, alite and C_3S are interchangeably used only in our LCA work. The GHG emissions associated with the electricity and fuel demand from the extraction of raw materials, grinding, blending, kilning, cooling, seed filtration, and mixing/batching were calculated based on the electricity grid of California.

A sensitivity analysis was performed by varying model input parameter values. These effects were assessed: 1) distance between extraction site of raw materials to a cement plant; 2) distance between the cement plant and a concrete mixing plant; 3) productivity/yield of seed from hydrating C_3S/alite; and 4) electricity input for filtration.

4. Results and discussions

4.1. Structure

Both C-S-H seeds show the typical XRD patterns (Fig. 2) for nanocrystalline C-S-H [39]. Typical impurities (i.e., $CaCO_3$ polymorphs or Ca$(OH)_2$) were below the detection limit of XRD. Slight shifts of peak positions were observed between the seeds (e.g., at d-spacing of ~12, 3.1, and 1.8 Å), suggesting their difference in lattice parameters (Table 1). The smaller basal spacing of HighCa was due to more positive-charged Ca to the negative-charged basal layers at higher Ca/Si [15] (1.41 vs. 1.01, see EDS results in Table 1). The higher Ca/Si of HighCa was attributed to less water dilution. The large basal spacing and lack of layer-stacking along the c-axis of LowCa suggests higher surface area, which is in good accordance with N_2 sorption results

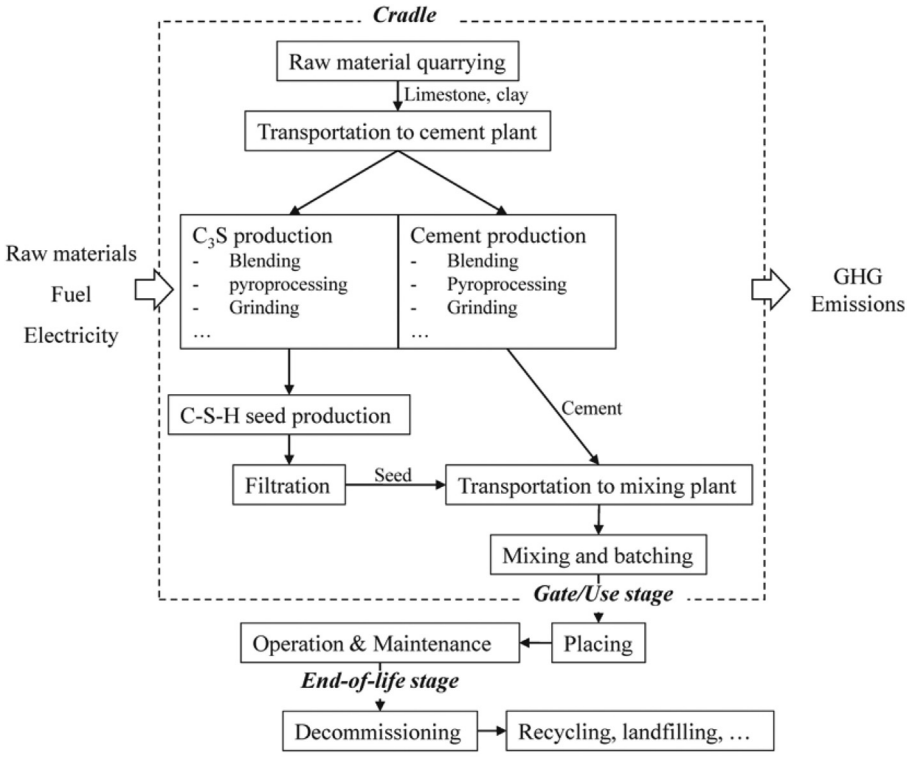

Fig. 1. The scope of assessment for seeded/unseeded cement pastes (dashed box): production of C_3S/alite and cement; transportation between raw materials extraction; and a cement plant and between cement and concrete plants.

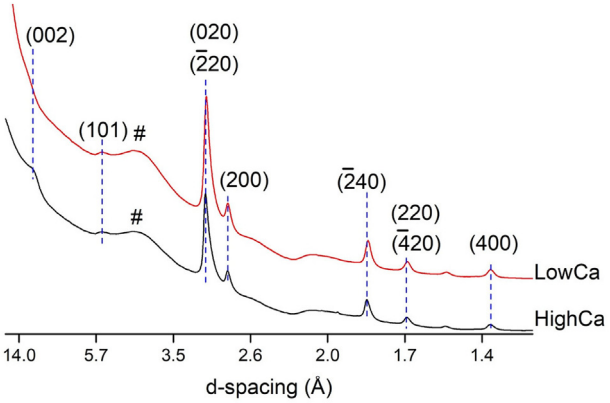

Fig. 2. XRD patterns of the seeds. # background of glassy capillary.

Table 1
Refinement of the lattice parameters, EDS results of Ca/Si, Ca concentration, and the BET surface area of the seeds.

Seed	a (Å)	b (Å)	c (Å)	γ (°)	Ca/Si	Ca (mmol/L)	Surface area (m^2/g)
LowCa	6.732	7.369	22.68	123.14	1.01	9.7	188
HighCa	6.707	7.333	21.82	123.14	1.41	21.3	162

(Table 1). The surface area of the seeds is ~1.5–2 times larger than of the C-S-H seeds synthesized in [21]. The observations agree with previous studies that hydrated C_3S typically presented an extremely high surface area, particularly in diluted systems [40,41].

HighCa presented two features in STXM images (Fig. 3A and B): foil-like fine structure for, possibly, precipitates from the solution and fibers on fringes of hydrated C_3S grains. LowCa seeds (Fig. 3D and E) only presented foils for both hydrated C_3S fringes and, possibly, precipitates. The foil-like C-S-H seeds resemble the morphology of nanocrystalline C-S-H synthesized via the lime-silica reaction [42,43]. High-resolution TEM images (Fig. 3C and F) confirmed the morphological features – the fibers are hundreds of nanometers long, and the nano-foils are crumpled. The morphology of C-S-H from hydrated C_3S is sensitive to the lime concentration. The high lime concentration (21.3 mmol/L, Table 1) of less diluted C_3S hydration results in the dual features of HighCa while the low concentration (9.7 mmol/L) of LowCa suspension leads to only the crumpled foils. The concentration-morphology correlation of the seeds agrees with [43], where the lime concentration threshold for fiber-foil features of hydrated C_3S was 22 mmol/L. No micro-crystallites (e.g., portlandite) were observed in many different regions of interest (ROIs) of the samples, consistent with our XRD results.

XANES spectra at Ca $L_{2,3}$-edge (Fig. 3G) of both seeds in different ROIs are all comparable, suggesting their similar Ca environments. The a_2 and b_2 peaks of the seeds positioned at higher energy than those of $Ca(OH)_2$ because Ca in the C-S-H seeds are mainly 7-fold coordinated while Ca in $Ca(OH)_2$ are 6-fold coordinated [15,44]. The energy differences between a_2 and a_1 peaks and b_2 and b_1 peaks are all ~1.1 eV, suggesting a higher degree of distortion from a perfect octahedral Ca—O coordination relative to portlandite (1.4 eV of energy differences) [45,46]. The highly distorted Ca—O coordination in the seeds is consistent with the Ca $L_{2,3}$-edge of C-S-Hs via lime-silica reaction, co-precipitation, and hydrated C_2S [27,45].

XANES spectra at O K-edge (Fig. 3H) of both seeds in different ROIs are also comparable, suggesting their similar O environments. The absence of a peak at ~543 eV (signature of portlandite [47]) suggests that the C-S-H seeds are portlandite-free. XANES spectra (Fig. 3I) show a 0.4 eV lower Si K-edge of HighCa relative to LowCa, suggesting that the polymerization degree of silicate chains in HighCa is lower than in LowCa (i.e., shorter silicate chains in HighCa). More Si was replaced with bridging Ca in HighCa for its high Ca/Si [48]. The negative correlation between Ca/Si and chain length is consistent with previous XANES [27,45,46], nuclear magnetic resonance [43,49], and Raman [50–52] results of C-S-Hs synthesized by various methods. The absence of shoulder at ~1844 eV suggests the absence of Q^3 and Q^4 in the seeds [53], namely no silica gel (secondary product) was observed.

4.2. Performance

Calorimetry results (Fig. 4) show the influence of C-S-H seeds on the hydration of cement. Cement with 0.5 wt% HighCa or LowCa showed comparable onset of the formation of C-S-H and portlandite from the silicate hydration at ~45 min. The onset of the silicate hydration of the reference cement in the absence of seeds was ~1 h longer. The seeds significantly accelerated the silicates hydration – the shoulder of silicates hydration occurred at least 4 h earlier than the reference. Although the silicate shoulders in both seeded samples occurred at ~3 h, the shoulder height of the HighCa seeded cement was 8% higher than that of the LowCa seeded cement. The two seeds showed a comparable acceleration of aluminate hydration by shifting the dominated peak to 2 h earlier and increasing peak height by ~9%. The acceleration of cement hydration is due to the high surface area of the seeds, which provide extra nucleation sites for new C-S-H and ettringite [19]. It is important that silicate peak appeared earlier than aluminate peak; otherwise, the over-accelerated aluminate hydration would suppress the silicate hydration and thus disturb the strength gain of seeded cement at the early age [54].

The acceleration degree of 0.5 wt%-seeded cement in the present study is higher than that of C-S-H seeded cement in other studies at the same dosage. The effect of 0.5 wt% seeds on cement hydration in the present study is comparable to those in studies where up to 2 wt% dosage was used [16,22]. Total generated heat during 48 h hydration of seeded cement was 10% higher than that of the reference. This result is promising because not all C-S-H seeds in existing literature [22] sustained the acceleration effect up to 48 h and especially that the seed dosage in the present study is only 0.5 wt%. Although the surface area of LowCa is higher than HighCa, the acceleration effect of HighCa is slightly greater after 9 h. A previous study reported that seeds (unknown morphology, very likely foil-like) with lower Ca/Si but higher surface area exhibited a more pronounced acceleration effect on cement hydration compared to the high Ca/Si counterpart, in which case the acceleration effect might be dominated by the surface area of the seeds. Another study reported that seeds at Ca/Si = 2 exhibited a stronger acceleration effect on PC hydration than the seeds at Ca/Si = 0.4 [20]. However, the influence of impurities (silica gel and/or portlandite) on the acceleration effect was not eliminated. Our study suggests that the phase-pure seed with fiber-foil dual features (HighCa) has a more pronounced acceleration effect than the foil-like seed (LowCa), despite the slightly lower surface area of HighCa.

Nicoleau et al. have extensively studied the morphology and acceleration efficiency of polymer-stabilized C-S-H seeds [35,55–57]. The morphology of co-precipitated C-S-H can be controlled by the addition of different polymers. Without polymer stabilization, the acceleration effect of C-S-H seeds was not observed, while the relative acceleration of stabilized seeds on PC ranged from 0.7 to 3 per g of C-S-H seeds. The relative acceleration of polymer-stabilized seeds reported in Wang et al. [22] was either ~1 or below 1/g of C-S-H seeds. In our study, the relative acceleration values of LowCa and HighCa are 4.5 and 4.9/g of C-S-H seeds, respectively, both are higher than that of polymer-stabilized seeds in Nicoleau et al. [35]. Note that one should be extra careful with the relative acceleration because the efficiency of C-S-H seeds also depends on the cement compositions [55]. The higher acceleration effect of HighCa may be attributed to the fibrillar morphology, which provides more open and orientated structures (as evidenced in Fig. 3) for further aggregation and growth of C-S-Hs than foil-like LowCa. This

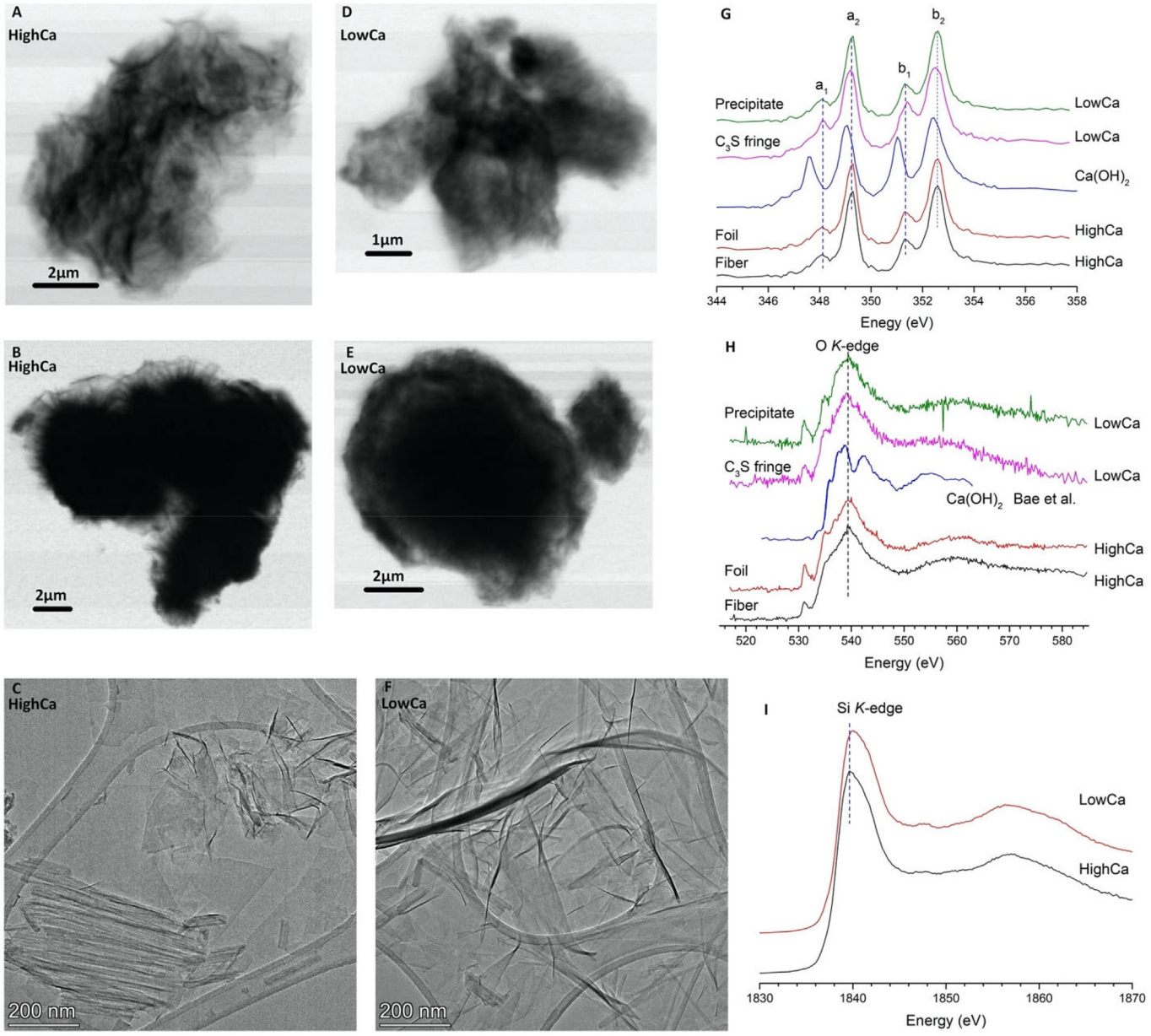

Fig. 3. A) and B) STXM image of HighCa seed taken at 356 eV; C) TEM image of HighCa; D) and E) STXM image of LowCa; F) TEM image of LowCa; G) and H) XANES spectra of seeds at different areas at Ca $L_{2,3}$- and O K- edges; I) bulk XANES spectra of seeds at Si K-edge.

observation is supported by the aggregation of polymer-stabilized seeds [35] and colloidal silica [58].

For each paste, three cubic (1040 × 1040 × 1040 μm^3) volume of interest (VOI)s were equally cropped from the reconstructed tomogram along with the height (shown in Fig. 5A as an example). A 3D bilateral filter (3 pixel size) [59] and a contrast enhancement with a saturated pixel of 0.35 were applied to eliminate noise and improve the contrast between different phases [60]. Threshold methods were applied to isolate anhydrous cement and pores of the pastes. Upper Otsu [61] algorithm provides segmented volumes in good agreement with observed anhydrous cement particles. For the pore network, statistical region merging (SRM) [62,63] algorithm achieved good segmentation results with the preservation of connectivity. Fig. 5B and C show the segmented anhydrous cement fraction and pore fraction, respectively, of the reference paste at 3 h. At the spatial resolution of 1.3 μm, the mean porosities of reference pastes with w/b = 0.5 at 3 h and 8 h were 15.9% and 12.2%, which fall in a reasonable range of porosity compared with a previous study. The porosity of 1d PC paste at the same spatial resolution and w/b in [64] is 11.5%. Note that the porosity determined by X-ray tomography is sensitive to the spatial resolution and the evolution of contrast resolution [64]. Lower resolution often results in higher porosity due to the lack of contrast between C-S-H and fine pores. Tomography with higher spatial resolution may not produce more reliable data. Typical X-ray tomography beamline that penetrates a high-volume of VOI of pastes with higher resolution (e.g., 0.5 μm) requires hours of data collection. Such a long time for data collection is not suitable for our in-situ study in the first hours. Seeded pastes exhibited a lower fraction of unreacted cement compared to the reference at the same age (Fig. 5D), confirming the acceleration effect of C-S-H seeds. At 3 h and 8 h, HighCa and LowCa exhibited similar acceleration degree, consistent with our calorimetry results—HighCa showed a slightly stronger acceleration effect after 9 h.

Fig. 6A shows the time of initial and final setting of pastes. With 0.5 wt% seeds, the initial and final setting times shifted to ~3 h and ~5 h earlier, respectively, relative to the reference. HighCa showed a slightly greater acceleration compared to the LowCa, evidenced by

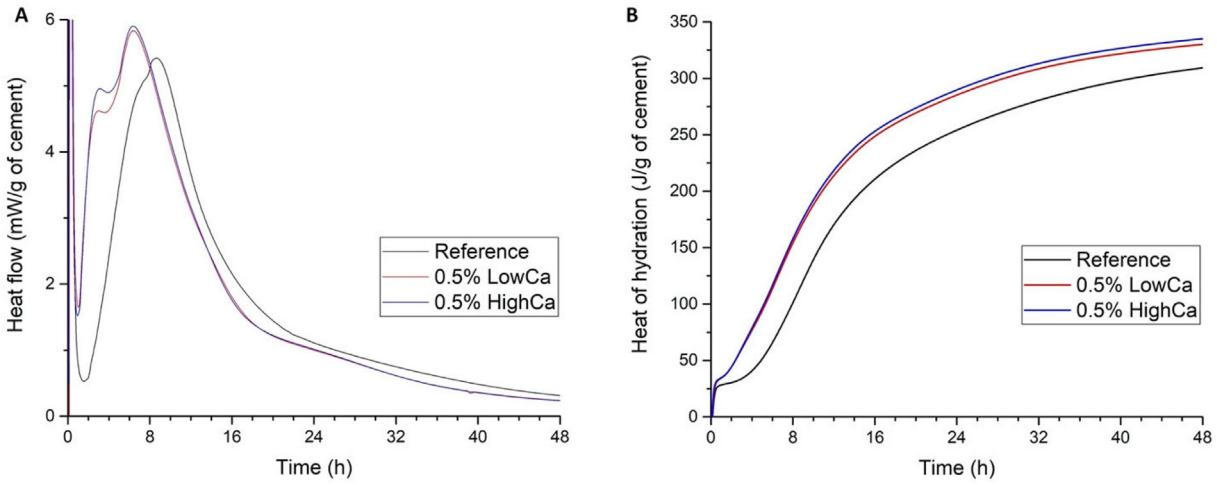

Fig. 4. A) Heat flow of pastes (w/b = 0.5); B) cumulative heat of hydration of pastes.

shortened initial and final setting by 15–20 min. The earliest setting of HighCa-seeded paste is consistent with our calorimeter results. Our setting time results confirm that the seed shape significantly influences the acceleration of cement hydration. The rapid initial setting induced by C-S-H seeds from C_3S hydration indicates their limitations in practice. The use of C-S-H seeds may be more practical in the manufacture of precast concrete than that of ready-mix concrete for the concern of workability. For the use of our C-S-H seeds in the ready-mix concrete industry, a lower dosage may be required to ensure workable seeded concrete. Alternatively, polymers can be used to improve the workability of C-S-H seeded cement-based materials. X-seed [65,66], *comb*-polymer stabilized plate-like C-S-H, has already been commercially available in the concrete industry. Future studies will consider the synergetic effects of polymer and our C-S-H seeds on the performance of seeded concrete.

The results of the compressive strength of pastes are consistent with our setting time results. At 1 day, seeded pastes showed two- to three-fold strengths compared to the reference. The acceleration effect of the seeds becomes less pronounced over time, but the strength development of seeded pastes was still ~20% higher than the reference at 28 days. The paste with 0.5 wt% HighCa exhibited higher and faster strength development than the LowCa counterpart. Apparently, the faster strength development of the HighCa group can be attributed to the more pronounced acceleration of cement hydration by HighCa. Seeded pastes presented considerably finer pore structures at 28 days compared to the reference. Both seeded pastes presented finer breakthrough radii than the reference—peak shifts from 40 nm to 13 nm. Compared to the reference, fewer large capillary pores with radius of 100–1000 nm appeared in the LowCa seeded paste, and the large capillary pores were not observed in the HighCa seeded paste. The finer pore structure of HighCa seeded paste contributed to its highest strength at 28 days. Micromechanics modelling has suggested that the compressive strength of cement pastes positively correlates to the degree of cement hydration and the gel-space ratio [67,68]. These modelling studies are consistent with our experimental results: the higher strength of HighCa group at 1–3 days relative to the reference can be attributed to the higher degree of hydration while the higher strengths of seeded groups at 28 days are due to the microstructure (gel-space) of pastes. The higher strength of HighCa group compared to LowCa group at all ages may be related to the reinforcement of fibrillar C-S-H, the role of which in micromechanics may be similar to nanotube/nanofiber [69,70].

Negligible strength improvement of seeded samples at 28 days was reported in [22], where seeds (platelet-like) were synthesized using the sol-gel method. John et al. [21] reported a higher strength of (lime-silica reacted C-S-H) seeded pastes at 28 days, and pastes with lower Ca/Si seeds showed a greater strength improvement than that of pastes with higher Ca/Si seeds. The strength development in John et al. [21] might be dominated by the surface area of the seed or the influenced polymerization of hydration product C-S-H. However, in the present study, HighCa seeds with slightly smaller surface area exhibited faster and higher strength development. Thus, it is very likely that the morphology of seeds is the dominating factor for the improvement in strength development. From the results, it is possible to lower the cement content in seeded PC-based materials to sustain comparable compressive strengths with the plain PC-based materials or to reduce the cross-section area of concrete elements in structural designs for equal capacity. Future studies will focus on the influences of C-S-H seeds with different Ca/Si ratios on the degree of polymerization of cement hydration, pore solution chemistry, and the nanostructure of C-S-H hydration product. In this study, we are more interested in validating the sustainable use of C-S-H seeds in PC pastes.

4.3. LCA

The energy consumptions and GHG emissions (CO_2-equivalent, CO_2-eq) of the production of C_3S/alite (Fig. 7A and B) are 7% and 12% higher than those of cement manufacturing, respectively (see SI for more details). The contributions of materials, energy, and transportation in C_3S and cement productions are similar. This is not surprising because 1) alite (impure-C_3S) is the primary compound in PC; 2) the intrinsic heat requirements of reaction for C_3S and PC clinker are similar (1.84 MJ/kg vs. 1.76 MJ/kg); and 3) the raw materials (i.e., limestone and quartz) for C_3S production can be obtained from the extraction site of clinker manufacturing. With seed dosages of 0.5 wt%, the energy consumptions and GHG emissions from the production of seeded pastes are only < 1% higher than the reference paste (Fig. 7C). The low dosage of C-S-H seeds and low impacts from C_3S production result in the negligible influences on the energy consumptions and GHG emissions of the paste productions.

CO_2-eq intensity (GHG emissions normalized to compressive strength) expresses the eco-performance of the pastes. The CO_2-eq intensity of seeded pastes was 2–3 times lower than that of reference paste at 1 day (Fig. 7D). 18% and 30% reductions in CO_2-eq intensity were observed for LowCa and HighCa seeded pastes at 28 days, respectively, relative to the reference. The eco-performance of HighCa seeded pastes outclassed the LowCa counterpart due to 1) higher compressive strength of HighCa seeded paste; and 2) slightly lower energy consumptions and GHG emissions of the HighCa production (higher productivity and lower C_3S demand).

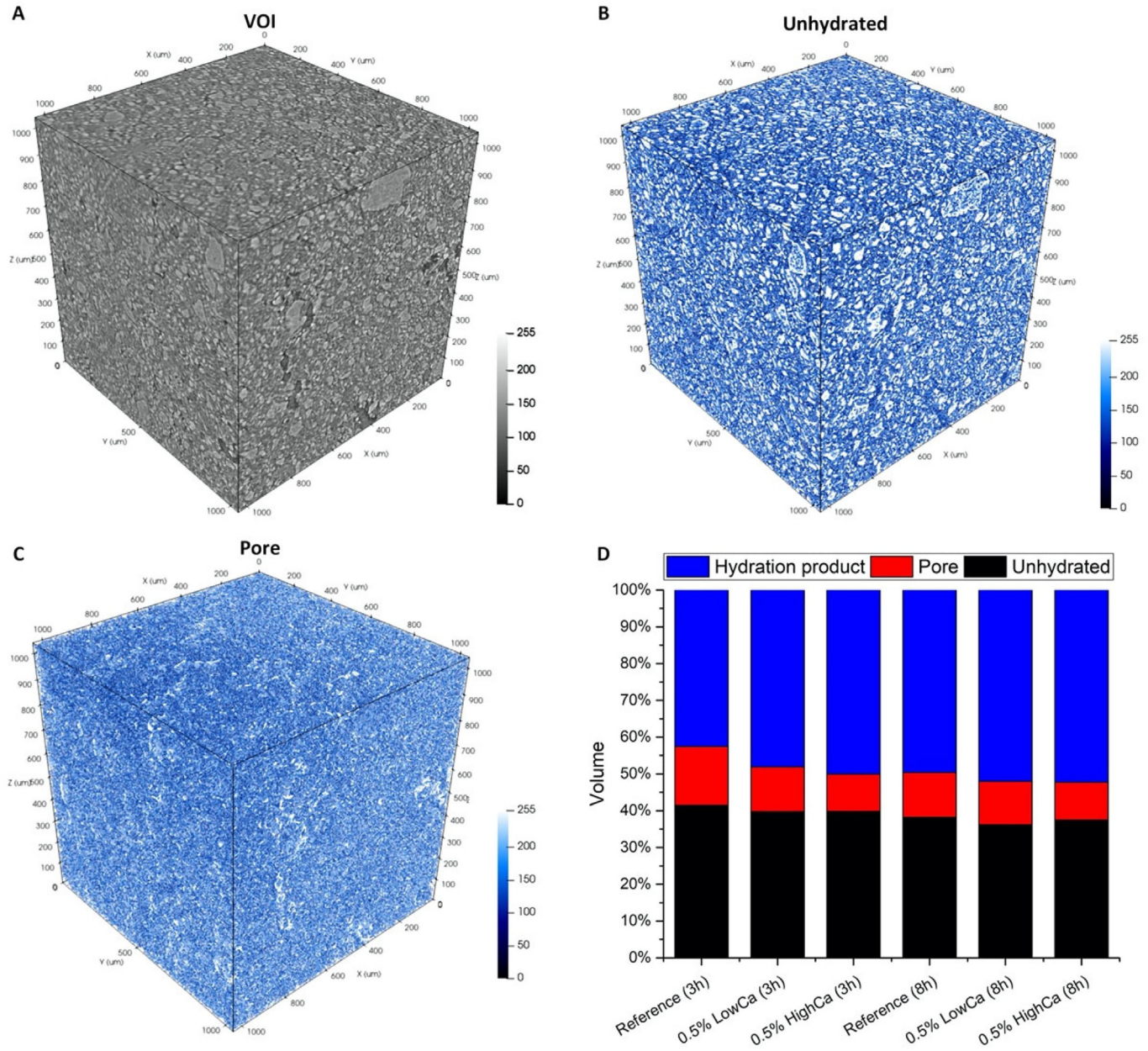

Fig. 5. A) A cubic VOI of reference paste at 3 h; B) segmented anhydrous cement grains of reference paste at 3 h; C) segmented pores of reference paste at 3 h of reference paste at 3 h; D) microstructure evolution of pastes at 3 h and 8 h.

Over 30% improvement in eco-performance of cement-based materials can be achieved with the use of supplementary cementitious materials (SCMs, e.g., fly ash) at 28 days [31]. However, fly ash blended cement may exhibit relatively low strengths at 28 day [2], thus resulting in longer curing or larger cross-sections of concrete elements in structural designs. These consequences compromise the goal of sustainable materials design and/or lead to a loss of industrial interests. Partial cement replacement with GBFS, silica fume, or diatomite can lower the energy consumptions and GHG emissions of cement-based materials production without compromising the early strength [72]. However, the production/reserves of silica fume and diatomite are very limited, and they are expensive [30]; the production of GBFS, although higher than silica fume and diatomite, still fails to meet the massive demand for cement [2]. Moreover, the supply of these SCMs is geographically not well distributed, meaning that the energy consumptions and environmental impacts are very sensitive to transportation [29].

C-S-H seeds prepared from C_3S/alite hydration present no such limitations or monetary concerns. Alite can be massively produced at cement plants. Thus, its energy consumptions and environmental impacts are not sensitive to transportation. Seeded pastes showed nearly identical sensitivity to transportation distance compared to the reference (see Fig. 7E). The GHG emissions of seeded paste production are slightly sensitive to the productivity of seeds (proportional to the required quantity of C_3S) but are not sensitive to the energy efficiency of filtration. Using belite/C_2S as the seed precursor possibly results in higher seed productivity due to the lower Ca content in C_2S (i.e., initial Ca/Si = 2 is closer to Ca/Si in HighCa C-S-H seeds). The lower intrinsic thermal requirement of formation (1.34 MJ/kg) and less Ca in C_2S also result in lower energy consumptions and GHG emissions during belite pyroprocessing. Note that C-S-Hs from diluted belite hydration are also fibrillar [45]. Thus, many evidences suggest that it is feasible to further lower the energy consumptions and GHG emission of seeded cement-based materials with belite-hydrated seeds.

Moreover, it is possible to collect fibrillar C-S-H seeds from hydrated

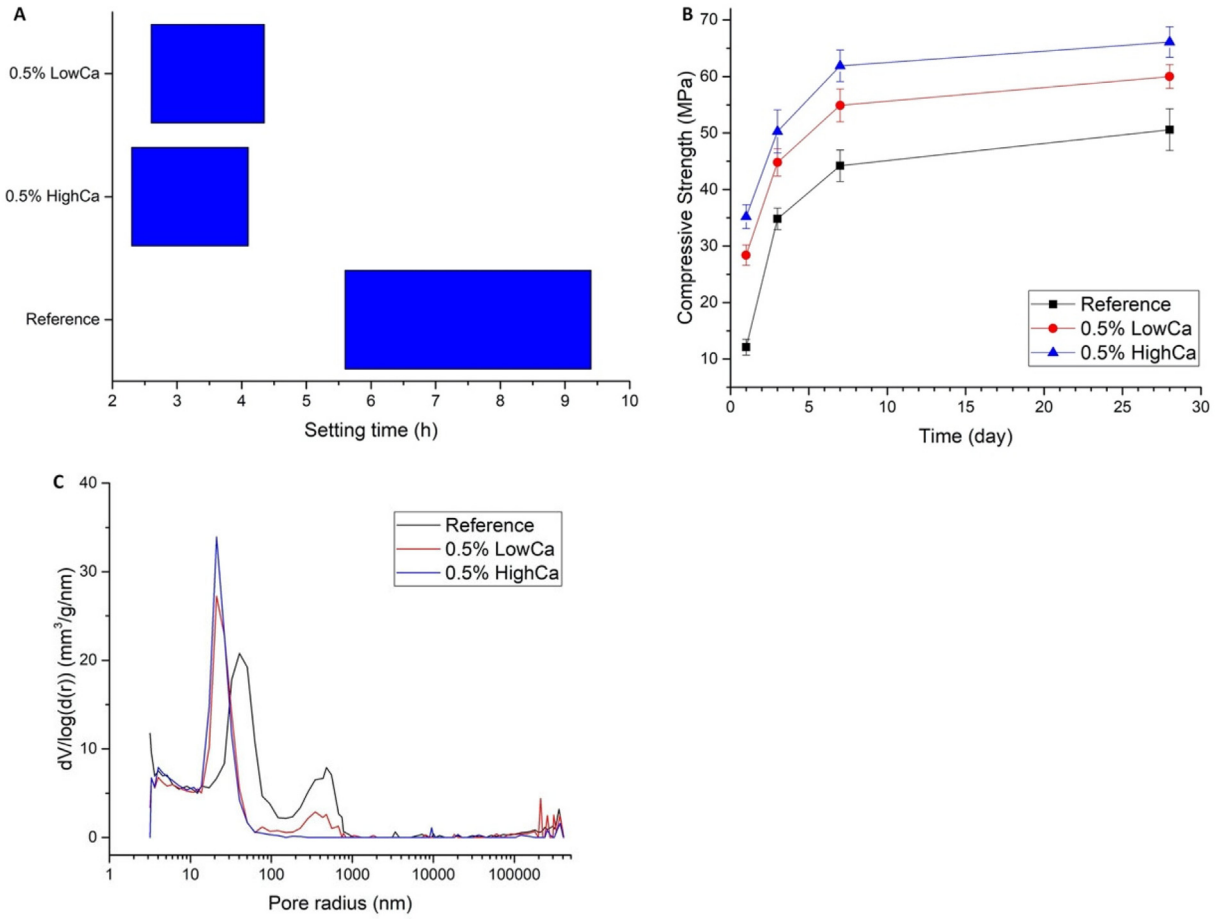

Fig. 6. A) Setting time of pastes; B) compressive strength of pastes at different ages; C) pore structure of pastes at 28 days.

cement. Typically, 1.4%–9% of fresh concrete is returned with ready-mix concrete trucks from every delivery [73], and the required water for washing-out is ~100 L/m^3 of truck capacity [74]. Thus, a large amount seeds could be available from reclaimed waste cement and wash water. It would be interesting to study C-S-H seeds from recycled fresh concretes, as they can be even more low-cost and sustainable [75]. The seed precursor used in our experimental work is pure triclinic C_3S. A TEM study showed that C-S-H fibers of pure triclinic C_3S after 1 day of hydration at w/b = 0.4 are thinner but have a similar length than Mg-doped monoclinic C_3S [76]. The morphological difference of C-S-Hs from highly diluted hydration of C_3S polymorphs (monoclinic and triclinic) is unclear. The influences of different elements (e.g., Mg, Al, Fe, and Na) on the morphology of C-S-Hs from diluted hydration of C_3S remain unknown. Future studies will focus on more practical utilization of C-S-H seeds from silicates hydration. The influences of C-S-H seeds from more practical seed precursors (e.g., alite and belite) with different dopants on the acceleration of PC will be considered.

5. Conclusions

Low-cost and largely available C-S-H seeds can be prepared by diluted alite/C_3S hydration. These seeds are phase-pure with high surface areas. Foil-fiber C-S-H can be prepared at high Ca/Si, while seeds at low Ca/Si are purely foil-like. Both HighCa- and LowCa-seeded pastes outperformed the reference. HighCa seed exhibited a slightly higher acceleration effect on cement hydration and faster and stronger strength development to cement pastes compared to foil-like seeds at low Ca/Si. The seed shape is a dominating factor for cement acceleration and strength development. C-S-H seeds significantly accelerate the initial and final setting of cement. The fast setting and high early strength of seeded cement may benefit prefabricated concrete or modular construction. The finer pore size distribution of seeded pastes may improve the impermeability and resistance to chemical attack during the service life. The higher strength at 28 days caused by seeds can lower the cement content in concrete for achieving comparable compressive strengths or can reduce the cross-section of concrete elements without compromising structural capacity. Both approaches are materials-saving and sustainable.

The energy demand and GHG emissions of the productions of cement and C_3S/alite (seed precursor) are comparable. Because of the low dosage of the seed, its production has negligible influences on energy consumptions and GHG emissions of seeded paste manufacturing. GHG emissions of seeded products are insensitive to transportation and not very sensitive to seed productivity. This study has great implications in developing C-S-H seeds from waste cement and wash water in the ready-mix concrete industry.

CRediT authorship contribution statement

Jiaqi Li: Conceptualization, Methodology, Formal analysis, Investigation, Validation, Visualization, Writing - original draft.**Wenxin Zhang:**Formal analysis, Visualization, Writing - review & editing.**Ke Xu:**Investigation, Formal analysis, Visualization, Writing - review & editing.**Paulo J.M. Monteiro:**Writing - review & editing, Supervision, Funding acquisition.

Declaration of competing interest

The authors declare that they have no known competing financial

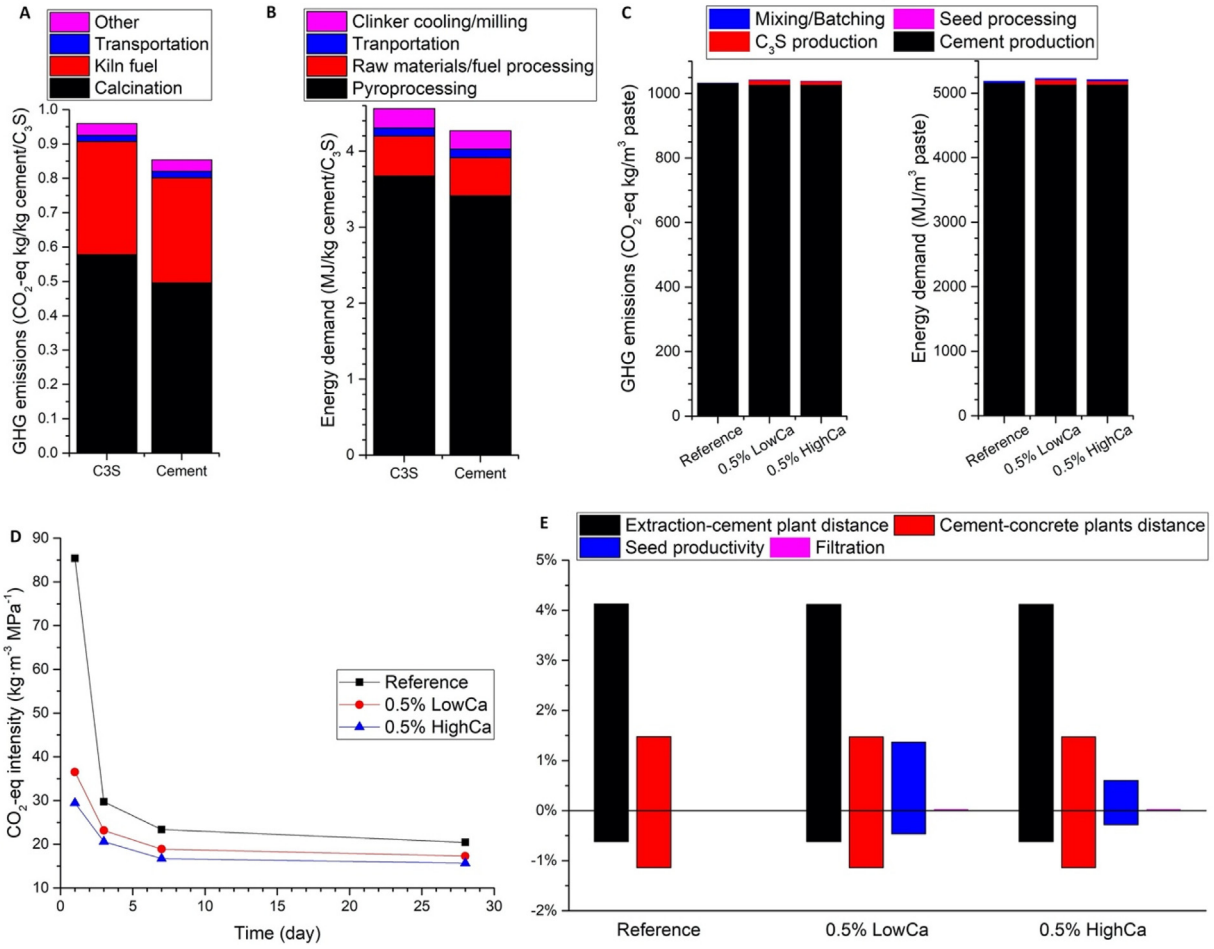

Fig. 7. A) Energy consumptions and B) GHG emissions of cement and C_3S production; C) energy consumptions and GHG emissions of paste productions; D) eco-performance of pastes (GHG emissions normalized by strengths); E) sensitivity analysis of GHG emissions from paste production by varying distance between materials extraction and cement plant (0–200 km), distance between cement and concrete plants (25–200 km), seed productivity (± 20%), and filtration efficiency (0.03–0.25 kWh/kg) [71].

interests or personal relationships that could have appeared to influence the work reported in this paper.

Acknowledgement

This work was funded by the Singapore National Research Foundation through a grant to the Berkeley Education Alliance for Research in Singapore (BEARS) for the Singapore-Berkeley Building Efficiency and Sustainability in the Tropics (SinBerBEST) Program. The Advanced Light Source is supported by the Director, Office of Science, and Office of Basic Energy Sciences of the U.S. Department of Energy under Contract No. DE-AC02-05CH11231. We acknowledge the Paul Scherrer Institut, Villigen, Switzerland for provision of synchrotron radiation beamtime at beamline PHOENIX of the SLS and would like to thank Dr. Thomas Huthwelker for assistance. We thank Prof. Claire White for the access to calorimeter in Princeton University. We thank Dr. Yaqiang Li at Beijing University of Technology for MIP measurement. We thank Qi Zheng for the assistance of TEM imaging.

Appendix A. Supplementary data

Supplementary data to this article can be found online at https://doi.org/10.1016/j.cemconres.2020.106195.

References

[1] P.J.M. Monteiro, S.A. Miller, A. Horvath, Towards sustainable concrete, Nat. Mater. 16 (2017) 698–699.
[2] M.C.G. Juenger, R. Snellings, S.A. Bernal, Supplementary cementitious materials: new sources, characterization, and performance insights, Cement Concrete Res 122 (2019) 257–273.
[3] S.A. Miller, Supplementary cementitious materials to mitigate greenhouse gas emissions from concrete: can there be too much of a good thing? J. Clean. Prod. 178 (2018) 587–598.
[4] M. Antoni, J. Rossen, F. Martirena, K. Scrivener, Cement substitution by a combination of metakaolin and limestone, Cem. Concr. Res. 42 (2012) 1579–1589.
[5] I. Diaz-Loya, M. Juenger, S. Seraj, R. Minkara, Extending supplementary cementitious material resources: reclaimed and remediated fly ash and natural pozzolans, Cement Concrete Comp 101 (2019) 44–51.
[6] K. Celik, C. Meral, M. Mancio, P.K. Mehta, P.J.M. Monteiro, A comparative study of self-consolidating concretes incorporating high-volume natural pozzolan or high-volume fly ash, Constr. Build. Mater. 67 (2014) 14–19.
[7] S.A. Miller, P.R. Cunningham, J.T. Harvey, Rice-based ash in concrete: a review of past work and potential environmental sustainability, Resour Conserv Recy 146 (2019) 416–430.
[8] K. Celik, C. Meral, A.P. Gursel, P.K. Mehta, A. Horvath, P.J.M. Monteiro, Mechanical properties, durability, and life-cycle assessment of self-consolidating concrete mixtures made with blended portland cements containing fly ash and limestone powder, Cement Concrete Comp 56 (2015) 59–72.
[9] B. Lothenbach, D. Nied, E. L'Hopital, G. Achiedo, A. Dauzeres, Magnesium and calcium silicate hydrates, Cement Concrete Res 77 (2015) 60–68.
[10] E. John, T. Matschei, D. Stephan, Nucleation seeding with calcium silicate hydrate - a review, Cement Concrete Res 113 (2018) 74–85.
[11] H. Manzano, J.S. Dolado, A. Guerrero, A. Ayuela, Mechanical properties of crystalline calcium-silicate-hydrates: comparison with cementitious C-S-H gels, Phys Status Solidi A 204 (2007) 1775–1780.
[12] D.S. Hou, T.J. Zhao, H.Y. Ma, Z.J. Li, Reactive molecular simulation on water

confined in the nanopores of the calcium silicate hydrate gel: structure, reactivity, and mechanical properties, J. Phys. Chem. C 119 (2015) 1346–1358.
[13] J.S. Dolado, M. Griebel, J. Hamaekers, A molecular dynamic study of cementitious calcium silicate hydrate (C-S-H) gels, J. Am. Ceram. Soc. 90 (2007) 3938–3942.
[14] J.S. Dolado, M. Griebel, J. Hamaekers, F. Heber, The nano-branched structure of cementitious calcium-silicate-hydrate gel, J. Mater. Chem. 21 (2011) 4445–4449.
[15] I.G. Richardson, Model structures for C-(A)-S-H(I), Acta Crystallogr B 70 (2014) 903–923.
[16] F. Wang, X.M. Kong, D.M. Wang, Q.B. Wang, The effects of nano-C-S-H with different polymer stabilizers on early cement hydration, J. Am. Ceram. Soc. 102 (2019) 5103–5116.
[17] G. Land, D. Stephan, The effect of synthesis conditions on the efficiency of C-S-H seeds to accelerate cement hydration, Cement Concrete Comp 87 (2018) 73–78.
[18] P. Bost, M. Regnier, M. Horgnies, Comparison of the accelerating effect of various additions on the early hydration of Portland cement, Constr. Build. Mater. 113 (2016) 290–296.
[19] J.J. Thomas, H.M. Jennings, J.J. Chen, Influence of nucleation seeding on the hydration mechanisms of tricalcium silicate and cement, J. Phys. Chem. C 113 (2009) 4327–4334.
[20] P.J.M. Monteiro, G.Q. Geng, D. Marchon, J.Q. Li, P. Alapati, K.E. Kurtis, M.J.A. Qomi, Advances in characterizing and understanding the microstructure of cementitious materials, Cement Concrete Res 124 (2019).
[21] E. John, J.D. Epping, D. Stephan, The influence of the chemical and physical properties of C-S-H seeds on their potential to accelerate cement hydration, Constr. Build. Mater. 228 (2019).
[22] F. Wang, X. Kong, L. Jiang, D. Wang, The acceleration mechanism of nano-CSH particles on OPC hydration, Construction Building Materials 249 (2020) 118734.
[23] K. Owens, M.I. Russell, G. Donnelly, A. Kirk, P.A.M. Basheer, Use of nanocrystal seeding chemical admixture in improving Portland cement strength development: application for precast concrete industry, Adv. Appl. Ceram. 113 (2014) 478–484.
[24] J. Ibanez, L. Artus, R. Cusco, A. Lopez, E. Menendez, M.C. Andrade, Hydration and carbonation of monoclinic C2S and C3S studied by Raman spectroscopy, J. Raman Spectrosc. 38 (2007) 61–67.
[25] C. Bagci, G.P. Kutyla, W.M. Kriven, Fully reacted high strength geopolymer made with diatomite as a fumed silica alternative, Ceram. Int. 43 (2017) 14784–14790.
[26] A. Ouzia, K. Scrivener, The needle model: a new model for the main hydration peak of alite, Cem. Concr. Res. 115 (2019) 339–360.
[27] S. Bae, R. Taylor, D. Hernandez-Cruz, S. Yoon, D. Kilcoyne, P.J.M. Monteiro, Soft X-ray spectromicroscopic investigation of synthetic C-S-H and C3S hydration products, J. Am. Ceram. Soc. 98 (2015) 2914–2920.
[28] K. Scrivener, R. Snellings, B. Lothenbach, A Practical Guide to Microstructural Analysis of Cementitious Materials, Crc Press, Boca Raton, 2016.
[29] S.A. Miller, R.J. Myers, Environmental impacts of alternative cement binders, Environ Sci Technol 54 (2020) 677–686.
[30] J.Q. Li, W.X. Zhang, C. Li, P.J.M. Monteiro, Green concrete containing diatomaceous earth and limestone: workability, mechanical properties, and life-cycle assessment, J. Clean. Prod. 223 (2019) 662–679.
[31] A.P. Gursel, H. Maryman, C. Ostertag, A life-cycle approach to environmental, mechanical, and durability properties of “green” concrete mixes with rice husk ash, J. Clean. Prod. 112 (2016) 823–836.
[32] J. Li, W. Zhang, C. Li, P.J.M. Monteiro, Eco-friendly mortar with high-volume diatomite and fly ash: performance and life-cycle assessment with regional variability, J. Clean. Prod. 261 (2020) 121224.
[33] S. Merlino, E. Bonaccorsi, T. Armbruster, The real structure of tobermorite 11 angstrom: normal and anomalous forms, OD character and polytypic modifications, Eur. J. Mineral. 13 (2001) 577–590.
[34] S. Mantellato, M. Palacios, R.J. Flatt, Impact of sample preparation on the specific surface area of synthetic ettringite, Cem. Concr. Res. 86 (2016) 20–28.
[35] L. Nicoleau, T. Gadt, L. Chitu, G. Maier, O. Paris, Oriented aggregation of calcium silicate hydrate platelets by the use of comb-like copolymers, Soft Matter 9 (2013) 4864–4874.
[36] A. MacDowell, D. Parkinson, A. Haboub, E. Schaible, J. Nasiatka, C. Yee, J. Jameson, J. Ajo-Franklin, C. Brodersen, A. McElrone, X-ray micro-tomography at the Advanced Light Source, Developments in X-ray Tomography VIII, International Society for Optics and Photonics, (2012), p. 850618.
[37] D. Gürsoy, F. De Carlo, X. Xiao, C. Jacobsen, TomoPy: a framework for the analysis of synchrotron tomographic data, J. Synchrotron Radiat. 21 (2014) 1188–1193.
[38] H.F.W. Taylor, Cement Chemistry, Thomas Telford, 1997.
[39] K. Garbev, G. Beuchle, M. Bornefeld, L. Black, P. Stemmermann, Cell dimensions and composition of nanocrystalline calcium silicate hydrate solid solutions. Part 1: synchrotron-based X-ray diffraction, J. Am. Ceram. Soc. 91 (2008) 3005–3014.
[40] H.M. Jennings, A model for the microstructure of calcium silicate hydrate in cement paste, Cem. Concr. Res. 30 (2000) 101–116.
[41] I. Odler, The BET-specific surface area of hydrated Portland cement and related materials, Cem. Concr. Res. 33 (2003) 2049–2056.
[42] J.Q. Li, G.Q. Geng, R. Myers, Y.S. Yu, D. Shapiro, C. Carraro, R. Maboudian, P.J.M. Monteiro, The chemistry and structure of calcium (alumino) silicate hydrate: a study by XANES, ptychographic imaging, and wide- and small-angle scattering, Cement Concrete Res 115 (2019) 367–378.
[43] E.T. Rodriguez, I.G. Richardson, L. Black, E. Boehm-Courjault, A. Nonat, J. Skibsted, Composition, silicate anion structure and morphology of calcium silicate hydrates (C-S-H) synthesised by silica-lime reaction and by controlled hydration of tricalcium silicate (C3S), Adv. Appl. Ceram. 114 (2015) 362–371.
[44] E. Gartner, I. Maruyama, J. Chen, A new model for the C-S-H phase formed during the hydration of Portland cements, Cement Concrete Res 97 (2017) 95–106.
[45] J.Q. Li, G.Q. Geng, W.X. Zhang, Y.S. Yu, D.A. Shapiro, P.J.M. Monteiro, The hydration of beta- and alpha(H)'-dicalcium silicates: an X-ray spectromicroscopic study, ACS Sustain. Chem. Eng. 7 (2019) 2316–2326.
[46] G.Q. Geng, R. Taylor, S. Bae, D. Hernandez-Cruz, D.A. Kilcoyne, A.H. Emwas, P.J.M. Monteiro, Atomic and nano-scale characterization of a 50-year-old hydrated C3S paste, Cement Concrete Res 77 (2015) 36–46.
[47] S. Bae, R. Taylor, D. Shapiro, P. Denes, J. Joseph, R. Celestre, S. Marchesini, H. Padmore, T. Tyliszczak, T. Warwick, Soft X-ray ptychographic imaging and morphological quantification of calcium silicate hydrates (C–S–H), J. Am. Ceram. Soc. 98 (2015) 4090–4095.
[48] E. L'Hopital, B. Lothenbach, D.A. Kulik, K. Scrivener, Influence of calcium to silica ratio on aluminium uptake in calcium silicate hydrate, Cement Concrete Res 85 (2016) 111–121.
[49] W. Kunther, S. Ferreiro, J. Skibsted, Influence of the Ca/Si ratio on the compressive strength of cementitious calcium-silicate-hydrate binders, J. Mater. Chem. A 5 (2017) 17401–17412.
[50] R.J. Kirkpatrick, J.L. Yarger, P.F. McMillan, P. Yu, X.D. Cong, Raman spectroscopy of C-S-H, tobermorite, and jennite, Adv. Cem. Based Mater. 5 (1997) 93–99.
[51] S. Ortaboy, J.Q. Li, G.Q. Geng, R.J. Myers, P.J.M. Monteiro, R. Maboudian, C. Carraro, Effects of CO2 and temperature on the structure and chemistry of C-(A-)S-H investigated by Raman spectroscopy, RSC Adv. 7 (2017) 48925–48933.
[52] K. Garbev, P. Stemmermann, L. Black, C. Breen, J. Yarwood, B. Gasharova, Structural features of C-S-H(I) and its carbonation in air - a Raman spectroscopic study. Part I: fresh phases, J. Am. Ceram. Soc. 90 (2007) 900–907.
[53] D. Cabaret, M. Le Grand, A. Ramos, A.M. Flank, S. Rossano, L. Galoisy, G. Calas, D. Ghaleb, Medium range structure of borosilicate glasses from Si K-edge XANES: a combined approach based on multiple scattering and molecular dynamics calculations, J. Non-Cryst. Solids 289 (2001) 1–8.
[54] D. Marchon, P. Juilland, E. Gallucci, L. Frunz, R.J. Flatt, Molecular and submolecular scale effects of comb-copolymers on tri-calcium silicate reactivity: toward molecular design, J. Am. Ceram. Soc. 100 (2017) 817–841.
[55] L. Nicoleau, The acceleration of cement hydration by seeding: influence of the cement mineralogy, ZKG international (Deutsch-englische Ausgabe. 1995) (2013) 40–49.
[56] L. Nicoleau, New calcium silicate hydrate network, Transport Res Rec (2010) 42–51.
[57] L. Nicoleau, Accelerated growth of calcium silicate hydrates: experiments and simulations, Cem. Concr. Res. 41 (2011) 1339–1348.
[58] A.C.J.H. Johnsson, M.C. Camerani, Z. Abbas, Combined electrospray-SMPS and SR-SAXS investigation of colloidal silica aggregation. Part I. Influence of starting material on gel morphology, J. Phys. Chem. B 115 (2011) 765–775.
[59] D. Ushizima, D. Parkinson, P. Nico, J. Ajo-Franklin, A. MacDowell, B. Kocar, W. Bethel, J. Sethian, Statistical segmentation and porosity quantification of 3d X-ray microtomography, Applications of Digital Image Processing XXXIV, International Society for Optics and Photonics, 2011, p. 813502.
[60] D. Ushizima, K. Xu, P.J. Monteiro, Materials data science for microstructural characterization of archaeological concrete, MRS Advances 5 (2020) 305–318.
[61] N. Otsu, A threshold selection method from gray-level histograms, IEEE Transactions on Systems, Man, and Cybernetics 9 (1979) 62–66.
[62] R. Nock, F. Nielsen, Statistical region merging, IEEE Trans. Pattern Anal. Mach. Intell. 26 (2004) 1452–1458.
[63] R. Nock, F. Nielsen, Semi-supervised statistical region refinement for color image segmentation, Pattern Recogn. 38 (2005) 835–846.
[64] E. Gallucci, K. Scrivener, A. Groso, M. Stampanoni, G. Margaritondo, 3D experimental investigation of the microstructure of cement pastes using synchrotron X-ray microtomography (μCT), Cem. Concr. Res. 37 (2007) 360–368.
[65] R. Reichenbach-Klinke, L. Nicoleau, Use of CSH Suspensions in Well Cementing, Google Patents, 2016.
[66] L. Nicoleau, G. Albrecht, K. Lorenz, E. Jetzlsperger, D. Fridrich, T. Wohlhaupter, R. Dorfner, H. Leitner, M. Vierle, D. Schmitt, Plasticizer-containing Hardening Accelerator Composition, Google Patents, 2014.
[67] B. Pichler, C. Hellmich, J. Eberhardsteiner, J. Wasserbauer, P. Termkhajornkit, R. Barbarulo, G. Chanvillard, Effect of gel-space ratio and microstructure on strength of hydrating cementitious materials: an engineering micromechanics approach, Cem. Concr. Res. 45 (2013) 55–68.
[68] B. Pichler, C. Hellmich, Upscaling quasi-brittle strength of cement paste and mortar: a multi-scale engineering mechanics model, Cem. Concr. Res. 41 (2011) 467–476.
[69] P. Hlaváček, V. Šmilauer, Fracture properties of cementitious composites reinforced with carbon nanofibers/nanotubes, Eng Mech 211 (2012) 391–397.
[70] V. Smilauer, P. Hlavacek, P. Padevet, Micromechanical analysis of cement paste with carbon nanotubes, Acta Polytech 52 (2012) 22–28.
[71] M. Huttunen, L. Nygren, T. Kinnarinen, B. Ekberg, T. Lindh, J. Ahola, V. Karvonen, A. Häkkinen, Specific energy consumption of vacuum filtration: experimental evaluation using a pilot-scale horizontal belt filter, Dry. Technol. 38 (2020) 460–475.
[72] P.K. Mehta, P.J. Monteiro, Concrete Microstructure, Properties and Materials, (2017).
[73] D.X. Xuan, C.S. Poon, W. Zheng, Management and sustainable utilization of processing wastes from ready-mixed concrete plants in construction: a review, Resour Conserv Recy 136 (2018) 238–247.
[74] P.K. Mehta, Reducing the environmental impact of concrete, Concr. Int. 23 (2001) 61–66.
[75] S.C. Kou, B.J. Zhan, C.S. Poon, Properties of partition wall blocks prepared with fresh concrete wastes, Constr. Build. Mater. 36 (2012) 566–571.
[76] A. Bazzoni, S.H. Ma, Q.Q. Wang, X.D. Shen, M. Cantoni, K.L. Scrivener, Effect of magnesium and zinc ions on the hydration kinetics of C3S, J. Am. Ceram. Soc. 97 (2014) 3684–3693.